

Supporting Information

Mechanistic study on Nitrogen-doped graphitic carbon-reinforced chromium nitride as durable electrocatalyst for oxygen reduction

Bidushi Sarkar, Arko Parui, Abhishek Kumar Singh and Karuna Kar Nanda*

*Materials Research Centre, Indian Institute of Science, Bangalore-560012, India

*Corresponding author: nanda@iisc.ac.in

MATERIALS AND METHODS

Chemicals

Dicyandiamide (DCDA, $C_2H_4N_4$) and chromium nitrate nonahydrate ($Cr(NO_3)_3 \cdot 9H_2O$), potassium hydroxide pellets (KOH), sulfuric acid (H_2SO_4) were purchased from Sigma Aldrich. Millipore water used was obtained from a Merck Milli-Q system. All chemicals used were used as received.

Material synthesis

Synthesis of CrN@NG-T: DCDA and Chromium nitrate were taken in a molar ratio of 5: 1 in a beaker to which 10 mL each of ethanol and DI water was added. The homogeneous solution was heated at 70 °C and dried. The powder was then collected, transferred to a quartz tube closed at one end, and subjected to pyrolysis in a tube furnace at a temperature $T = 700$ to 1000 °C. The as collected samples were named NG-700, CrN@NG-T ($T = 800, 900,$ and 1000) with an experimental yield of ~ 94 mg.

Synthesis of chromium oxide: A control sample in the absence of DCDA was synthesized following the similar procedure mentioned for the synthesis of CrN@NG-T. The sample as obtained was named as Cr_2O_3 .

Material characterization

The X-ray diffraction (XRD) data were collected on a wide-angle X-ray diffractometer (XRD, PANalytical) with Cu $K\alpha$ radiation (1.54 Å). Raman spectra were recorded on a WITec system

(excitation wavelength, 532 nm). Thermogravimetric analyses (TGA) were carried out on a PerkinElmer model TGA Q50 V20.13 Build 39. X-ray photoelectron spectroscopy (XPS) was obtained using ESCALAB 250, Thermo Scientific (monochromatic Al K α source, 1486.6 eV). The Brunauer-Emmett-Teller (BET) surface area was evaluated using Quantachrome Instruments, Autosorb iQ. The scanning electron microscopy (SEM) images and energy-dispersive X-ray spectroscopy (EDX) were obtained using a FESEM FEI Inspect 50. Transmission electron microscopy (TEM) images, high-resolution TEM (HRTEM) images, high-angle annular dark-field imaging - scanning transmission electron microscopy (HAADF - STEM), selected area electron diffraction (SAED) pattern and elemental mapping were obtained using FEI Titan Themis 300 (accelerating voltage = 300 kV). Inductively coupled plasma mass spectroscopy (ICP-MS) was done using a quadrupole ICPMS, Thermo X Series II. As the sample contains carbon, pre-treatment is done using wet digestion method as reported earlier^[1-2] before recording the ICP-MS results.

Electrochemical measurements

The electrochemical measurements were performed on CH Instruments (CHI 750E) workstation with a three-electrode cell using a rotating disk electrode (RDE). Glassy carbon electrode (GCE, area 0.07 cm²) and graphite rod were used as working and counter electrodes, respectively. Ag/AgCl and Hg/HgO electrodes were used as a reference electrode in acidic and alkaline medium, respectively. A comparison of the ORR activity for the as-synthesized catalysts is made with commercial 20 wt % Pt/C (purchased from Johnson Matthey Co., HiSPEC™ 3000). The potentials measured against the reference electrode were converted to potentials versus reversible hydrogen electrode (RHE) using the following formula, $E_{RHE} = E^{\circ}_{Ag/AgCl} + E_{Ag/AgCl} + 0.059 \text{ pH}$, where $E^{\circ}_{Ag/AgCl} = 0.197 \text{ V}$ and $E_{RHE} = E^{\circ}_{Hg/HgO} + E_{Hg/HgO} + 0.059 \text{ pH}$, where $E^{\circ}_{Hg/HgO} = 0.098 \text{ V}$.

The catalyst ink was prepared by weighing 4 mg of catalyst and adding 300 μL of ethanol, 200 μL of DI water and 5 wt % Nafion 117 solution (30 and 10 μL in alkaline and acidic electrolyte, respectively). The as-prepared ink (CrN@NG-T and Pt/C) was sonicated for 30 minutes and 2 μL of the ink was added onto GCE (catalyst loading, 0.21 mg cm⁻²) and air-dried.

The oxygen reduction reaction (ORR) measurements were carried out in 0.1 M KOH and 0.5 M H₂SO₄. The linear sweep voltammetry (LSV) was carried out at various rotation speeds ranging from 600 to 2200 rpm at a scan rate of 10 mV/s in an O₂ saturated solution. The cyclic voltammetry (CV) was carried out at a rotation speed of 600 rpm. The methanol tolerant studies were carried out in an O₂ saturated solution with 1 M methanol and 0.1 M KOH/ 0.5 M H₂SO₄ solution. The Koutechy- Levich (K-L) equation relates the J (total current density), J_k (kinetic current density), and J_L (diffusion-limiting current density) as,

$$1/J = 1/J_K + 1/J_L \quad (1)$$

The number of electrons transferred during ORR is calculated by Levich equation,

$$J_L = (0.62 n F D_{O_2}^{2/3} \nu^{-1/6} C_{O_2}) \omega^{1/2} \quad (2)$$

where n is the number of electrons transferred in the ORR process, F (Faraday constant) = 96485 C/mol, D_{O_2} is the bulk diffusion coefficient of oxygen in the electrolyte, ν is the kinematic viscosity of the electrolyte, C_{O_2} is the concentration of oxygen dissolved in the electrolyte, and ω is the angular velocity of the working electrode.

The mechanistic studies were done using a rotating ring disk electrode (RRDE, 0.196 cm²) as the working electrode. The catalyst ink preparation was similar as mentioned above but the amount of ink (CrN@NG-T and Pt/C) added to RRDE was 5 μ L (catalyst loading 0.19 mg cm⁻²). The peroxide yield (H₂O₂ %) and number of electrons transferred (n) and were estimated from the ring (I_R) and disk current (I_D) acquired from the rotating ring disk electrode (RRDE) profile at 1400 rpm using the following equations,^[3-4]

$$n = 4 N I_D / (N I_D + I_R) \quad (3)$$

$$\% \text{HO}_2^- = 200 I_R / (N I_D + I_R) \quad (4)$$

where N is the current collection efficiency of RRDE = 0.37

Computational details

Density functional theory (DFT) calculations were done with Vienna ab initio simulation (VASP) package.^[5] The Electron-ion interactions were described using the all-electron projector augmented wave pseudopotentials^[6], and Perdew-Bruke-Ernzehofer (PBE) generalized gradient approximation (GGA)^[7] was used to approximate the electronic exchange and correlations with an on-site effective Hubbard ($U_{\text{eff}} = U - J = 3$ eV) parameter was used for the Cr-4d states in DFT + U method as introduced by Dudarev et al. ^[8]. The Brillouin zone was sampled using a 2 \times 2 \times 1, 2 \times 2 \times 1, and 3 \times 2 \times 1 Monkhorst-Pack k-grid for NG, CrN, and CrN@NG, respectively. All structures were relaxed using a conjugate gradient scheme until the energies and each component of the forces converged to 10⁻⁵ eV and 0.01 eV \AA^{-1} , respectively. The optimized lattice parameters of hexagonal graphene were found to be $a=b=2.47$ \AA , in agreement with the previous reports^[9]. The hexagonal graphene cell was converted into a rectangular one. For making the structure of N doped graphitic carbon, at first a 2 \times 5 \times 1 supercell of the rectangular unit cell was taken. Then one carbon atom was replaced with one nitrogen atom. CrN bulk structure was taken from materials project database and optimized. The optimized lattice parameters were $a=b=c=4.25$ \AA . (111) and (200) surfaces were created, where the cell parameters are $a=6.01$ \AA , $b=10.41$ \AA and $a=b=4.25$ \AA , respectively. Subsequently, the (111) hexagonal system was converted to a

tetragonal system and optimized. Surface energies were calculated. The (200) surface having more stable surface ($\gamma = -1.62$ eV) was considered for further calculations over (111) surface ($\gamma = -0.911$ eV). The theoretical facet (200) is consistent with the exposed facet in the material as observed experimentally (as evident from XRD and HR-TEM studies). A $2 \times 3 \times 1$ supercell was considered and relaxed ($a=8.50$ Å and $b=12.75$ Å). With 3.52% lattice mismatch between NG and CrN (200) surface, heterostructure was created and optimized.

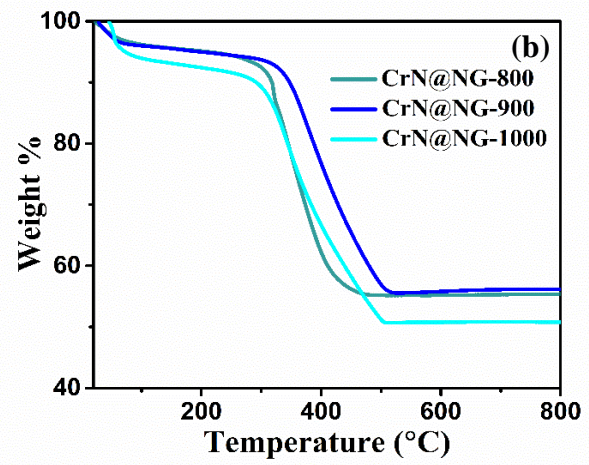
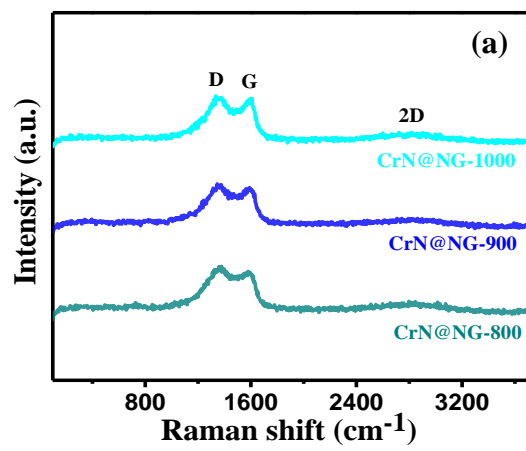


Figure S1 (a) Raman spectra. (b) TGA in O_2 atmosphere of as-synthesized samples.

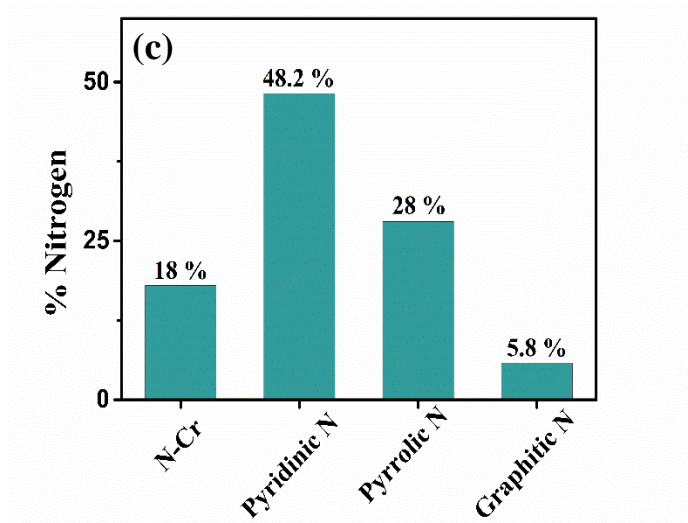
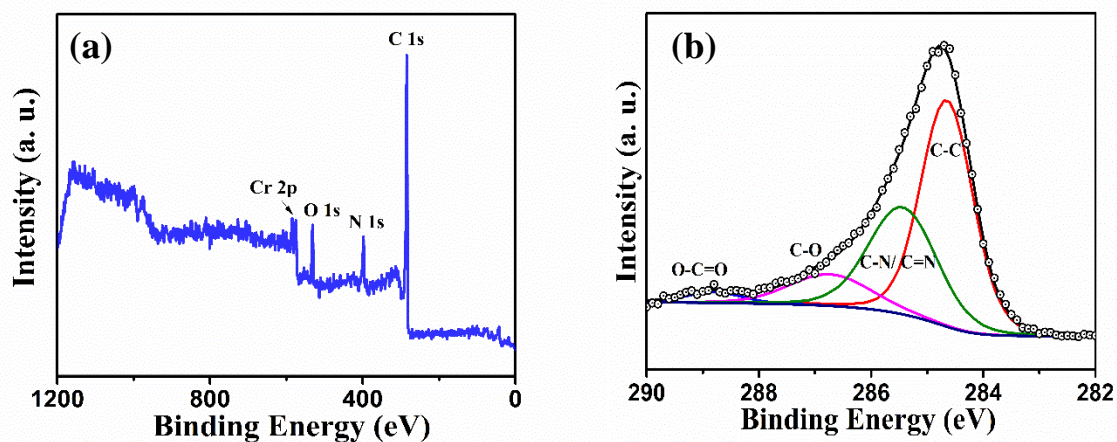


Figure S2 (a) Survey spectrum. (b) HRXPS of C 1s. and (c) % N content of each type in N 1s of CrN@NG-900.

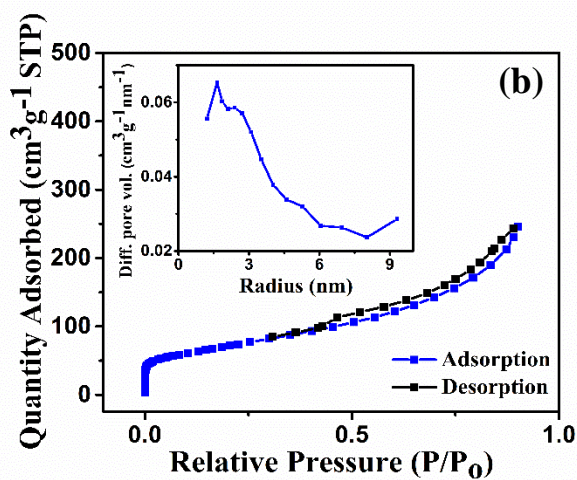
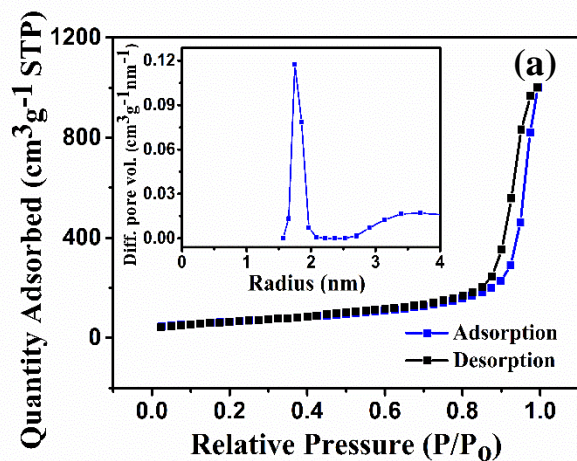


Figure S3 BET surface area N_2 adsorption/desorption isotherm and BJH plot to determine the pore radius of (a) CrN@NG-800. and (c) CrN@NG-1000

Table S1. N_2 adsorption-desorption analysis using BET method

	Specific surface area (m^2/g)	Average pore size (radius, nm)
CrN@NG-800	267.1	1.7
CrN@NG-900	249.5	1.64
CrN@NG-1000	244.8	1.62

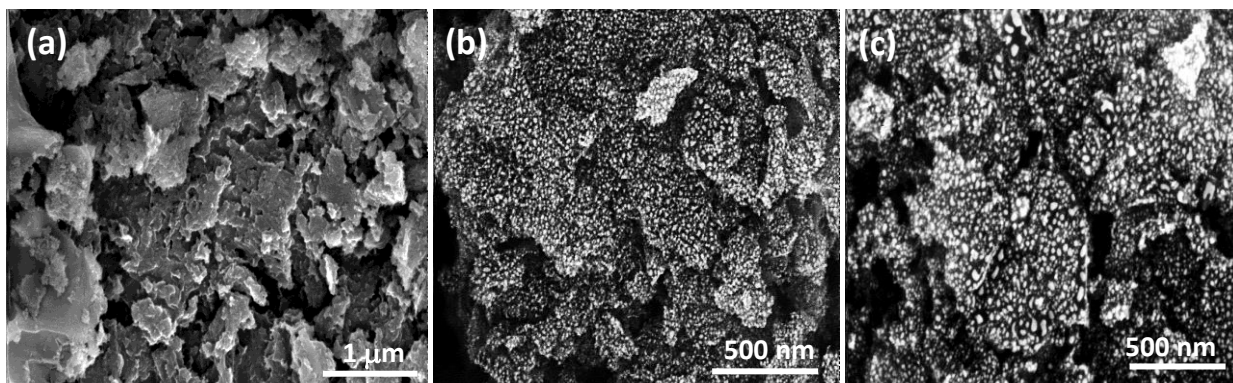


Figure S4 SEM image of (a) NG-700. (b) CrN@NG-800. (c) CrN@NG-1000

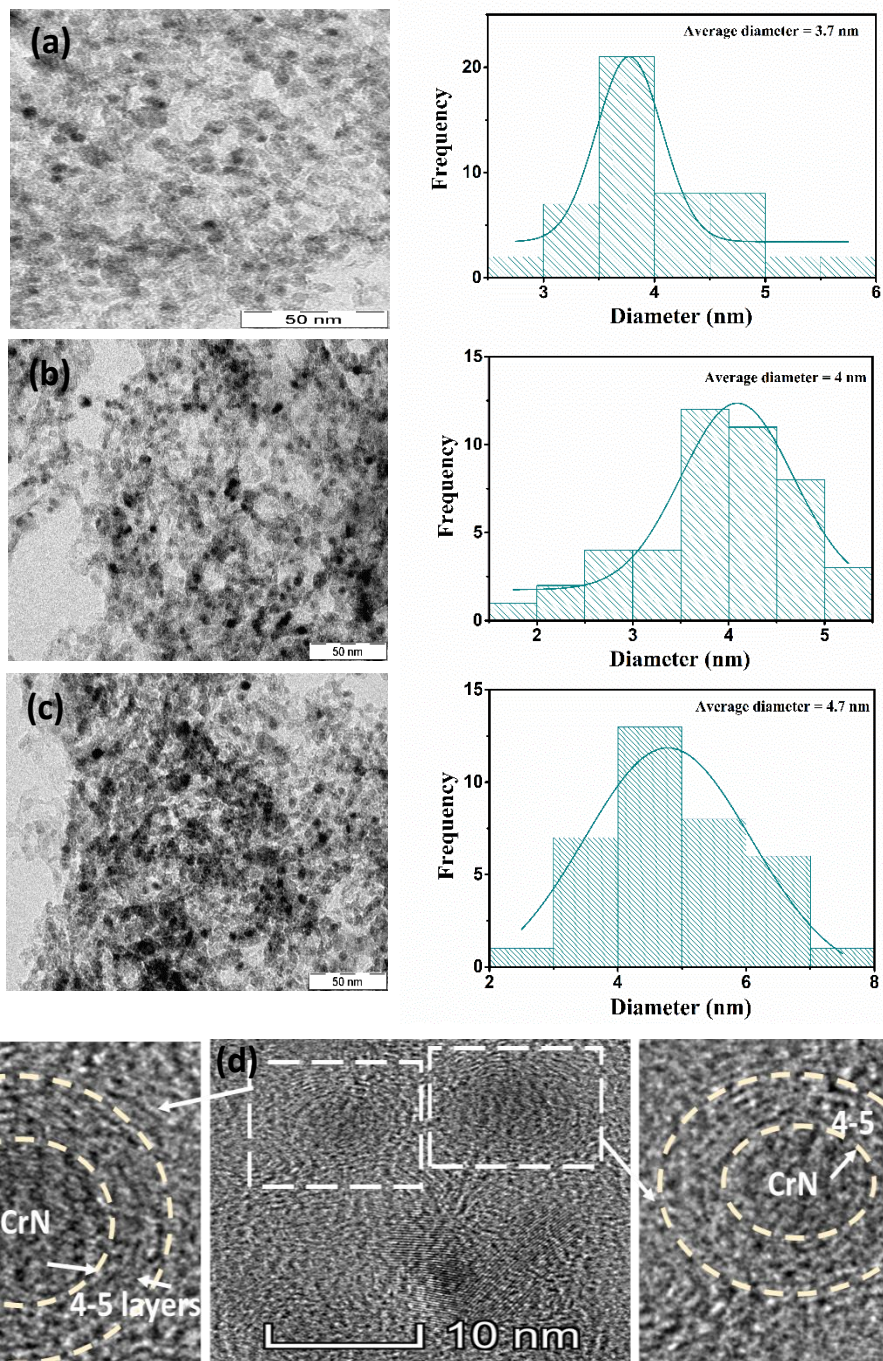


Figure S5 TEM image and corresponding particle size distribution curve of (a) CrN@NG-800. (b) CrN@NG-900. (c) CrN@NG-1000. (d) HRTEM of CrN@NG-1000 depicting the CrN nanoparticles encapsulated in 4-5 layers of graphitic carbon

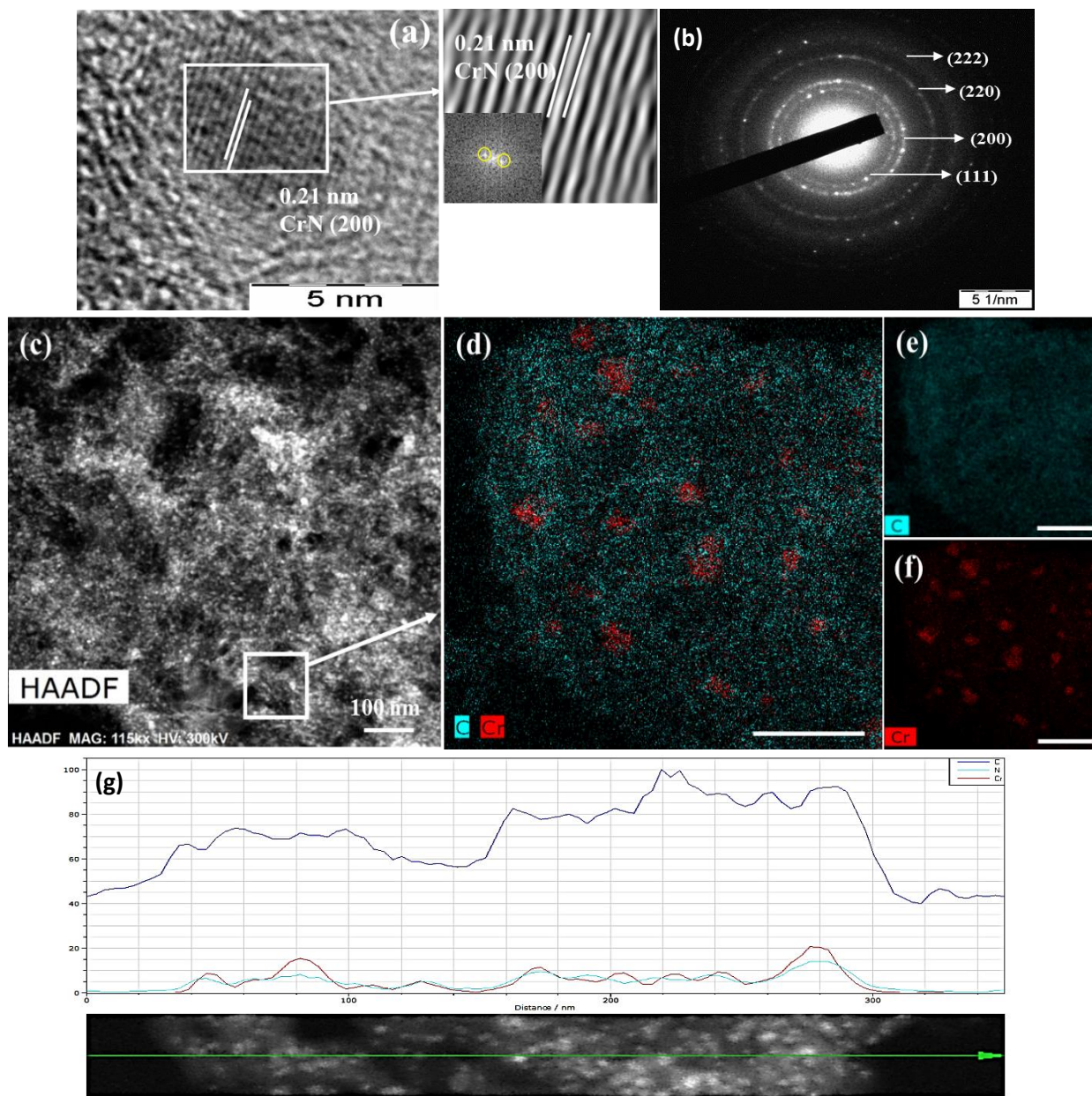


Figure S6 (a) HRTEM image, inset IFFT and FFT, (b) SAED pattern (c) HAADF-STEM image, (d) Overlapped mapping of C and Cr (Scale 30 nm), Mapping of (e) C, (f) Cr and (g) EDS line scan of CrN@NG-900.

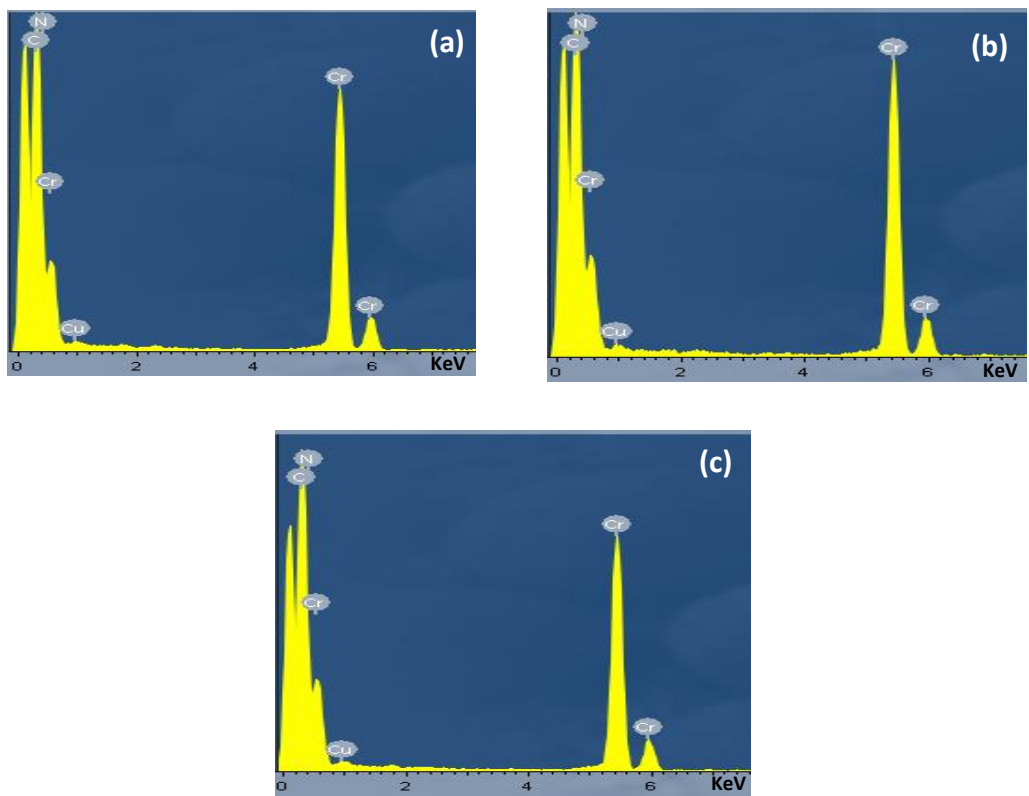


Figure S7 EDX spectra of (a) CrN@NG-800, (b) CrN@NG-900 and (c) CrN@NG-1000

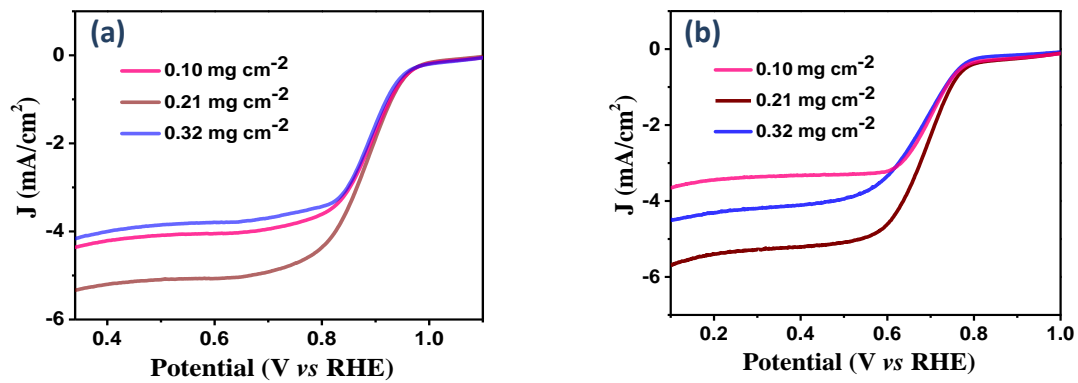


Figure S8. LSV polarisation curve of CrN@NG-900 (at 1600 rpm and 10 mVs⁻¹) with different catalyst loading in O₂ sat (a) 0.1 M KOH and (b) 0.5 M H₂SO₄

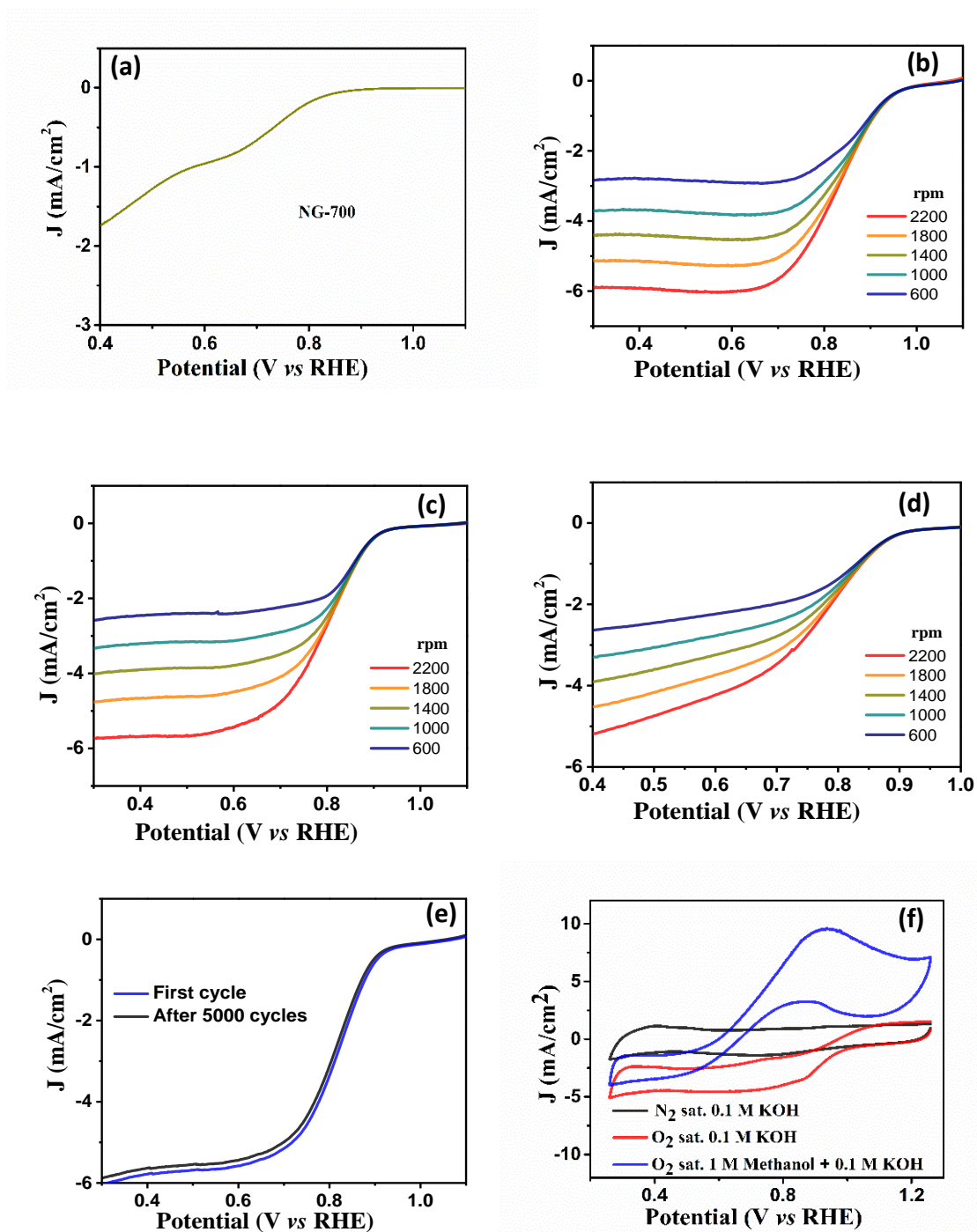


Figure S9 (a) LSV curve of NG-700 at a rotation speed of 1400 rpm and scan rate of 10 mV/s. RDE polarization curve at rotation rate ranging from 600 to 2200 rpm, scan rate 5 mV/s for (b) Pt/C, (c) CrN@NG-800, (d) CrN@NG-1000, in 0.1 M KOH. (e) ADT done at a scan rate of 100 mV/s and rotation rate of 1600 rpm in the potential range of 1.1 – 0.4 V to determine the cyclic stability of CrN@NG-900 after 5000th continuous cycles in 0.1 M KOH solution (O_2 sat) and (f) CV at 600 rpm at a scan rate of 5 mV/s in N_2 , O_2 saturated and on the addition of 1 M Methanol for Pt/C.

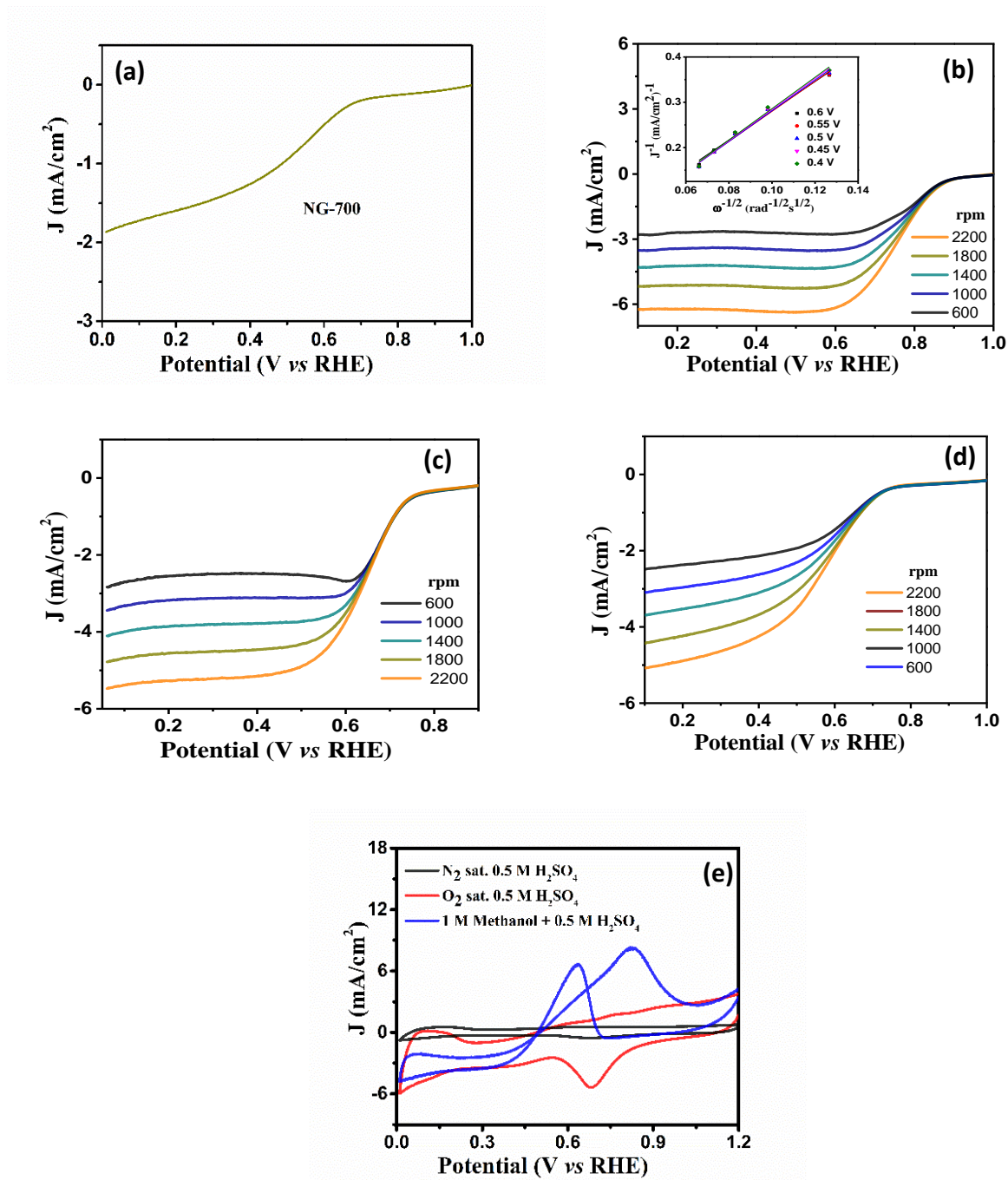


Figure S10 (a) LSV curve of NG-700 at a rotation speed of 1400 rpm and scan rate of 10 mV/s. RDE polarisation curve at rotation rate ranging from 600 to 2200 rpm, scan rate 5 mV/s for (b) Pt/C, (c) CrN@NG-800, (d) CrN@NG-1000, in 0.5 M H₂SO₄. and (e) CV at 600 rpm at a scan rate of 5 mV/s in N₂, O₂ saturated and on addition of 1 M Methanol for Pt/C.

Table S2 Values of limiting current density (J_L) at 0.4 V, kinetic current density (J_K) and mass activity for the catalysts in 0.1 M KOH solution

Catalyst	J_L (mA/cm ²)	J_K (mA/cm ²)		Mass activity (mA/mg)	
		At 0.90 V	At 0.85 V	At 0.90 V	At 0.85 V
CrN@NG-800	4.7	0.43	1.91	2.18	9.56
CrN@NG-900	5.3	0.74	3.19	3.71	16.0
CrN@NG-1000	4.3	0.20	0.98	1.04	4.90
Pt/C	5.6	1.59	5.45	7.9	27.25

Table S3 Values of limiting current density (J_L) at 0.3 V, kinetic current density (J_K) and mass activity for the catalysts in 0.5 M H₂SO₄ solution

Catalyst	J_L (mA/cm ²)	J_K (mA/cm ²)		Mass activity (mA/mg)	
		At 0.85 V	At 0.80 V	At 0.85 V	At 0.80 V
CrN@NG-800	4.5	0.33	0.66	1.66	3.32
CrN@NG-900	4.9	0.50	1.20	2.53	6.04
CrN@NG-1000	3.9	0.17	0.36	0.88	1.80
Pt/C	5.6	3.54	8.65	17.71	43.27

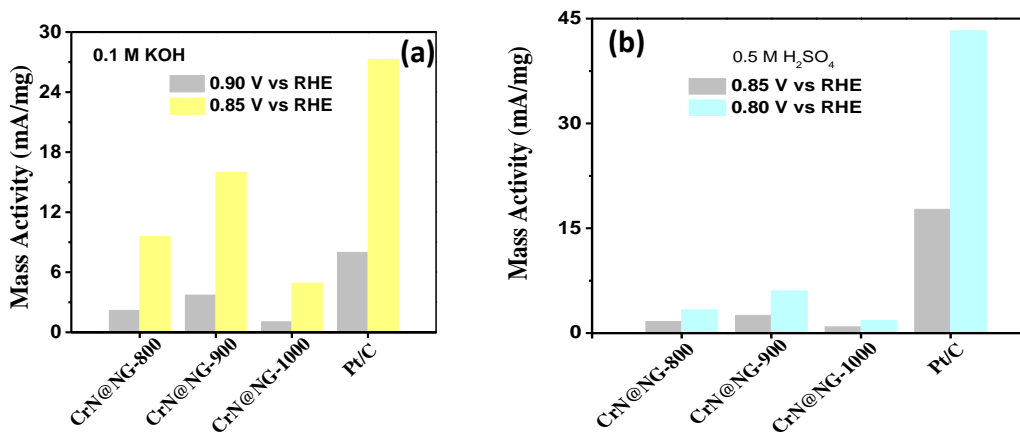


Figure S11. Mass activity (MA in mA/mg) of the as-synthesized catalysts and commercial Pt/C in 0.1 M KOH and 0.5 M H₂SO₄

Table S4 Comparison of the MA of as-synthesized catalyst with other nitride-based hybrids and carbon-supported materials

Catalyst	Loading (mg cm ⁻²)	Electrolyte (Reaction media)	Mass activity in mA/mg	Reference
CrN@NG-900	0.21	0.1 M KOH	16.0 (0.85 V)	This work
CrN@NG-900	0.21	0.1 M KOH	3.7 (0.90 V)	This work
MoCo-O-N/C	0.70	0.1 M KOH	0.39 (0.85 V)	[10]
V _{0.95} Co _{0.05} N	0.12	0.1 M KOH	3.7 (0.85 V)	[11]
Ni ₃ N/NiO	0.15	0.1 M KOH	5.2 (0.85 V)	[12]
Ti-Ni-N/C	0.5	0.1 M KOH	5.1 (0.85 V)	[13]
CrN@NG-900	0.21	0.5 M H₂SO₄	6.04 (0.80 V)	This work
FePc/C	0.6	0.1 M H ₂ SO ₄	2.22 (0.75 V)	[14]
BPNDC	-	1 M HClO ₄	6.0 (0.6 V)	[15]
Pd/NG	0.5	0.5 M H ₂ SO ₄	9.05 (~ 0.73 V)	[16]

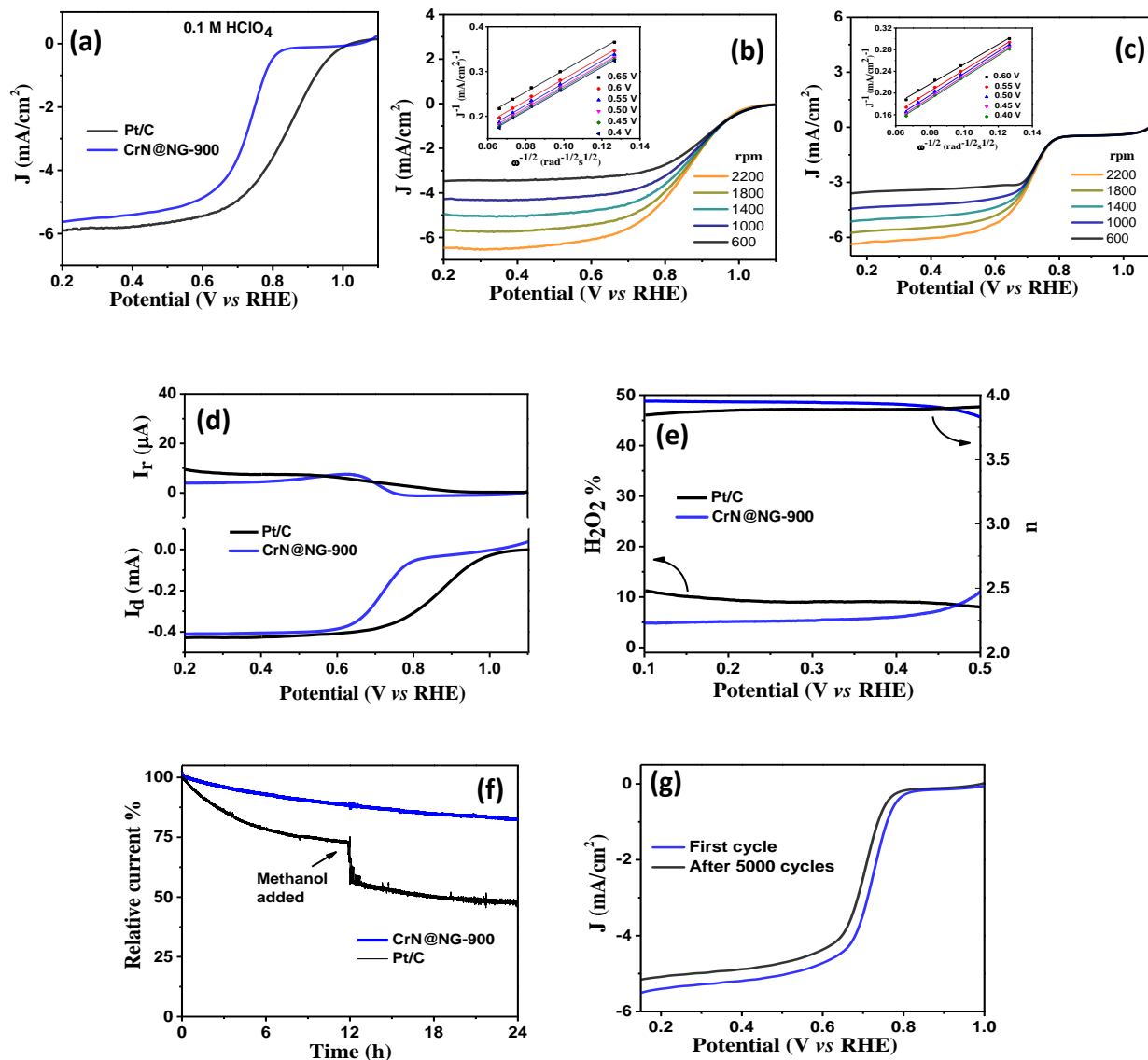


Figure S12 (a) Comparison of LSV for CrN@NG-900 and commercial Pt/C at a rotation speed of 1600 rpm and a scan rate of 10 mV/s in O₂ saturated 0.1 M HClO₄ solution obtained using RDE, LSV of (b) Pt/C, (c) CrN@NG-900 at different rotation speeds from 600 to 2200 rpm. Inset: KL plot (d) Ring current (I_r) and disk current (I_d) for CrN@NG-900 and Pt/C obtained using RRDE. (e) Percentage of H₂O₂ generation and number of electrons transferred. (f) Chronoamperometry study of CrN@G-900 and Pt/C for 24 h and methanol poisoning test in 1 M methanol done at around 12 h indicated by an arrow. (g) ADT done at a scan rate of 100 mV/s and rotation rate of 1600 rpm in the potential range of 1.0 – 0.1 V to determine the cyclic stability of CrN@NG-900 after 5000nd continuous cycles in 0.1 M HClO₄ solution (O₂ sat).

Table S5 Comparison of catalytic activity of the catalysts towards ORR with other recently reported nitrides in alkaline (KOH) and acidic (H_2SO_4 and $HClO_4$) media

Catalyst	Medium	Loading ($mg\ cm^{-2}$)	E_{onset} (V vs RHE)	$E_{1/2}$ (V vs RHE)	Stability % (Time (h))	Reference
CrN@NG-900	0.1 M KOH	0.21	0.96	0.85	88.6 (22)	This work
$V_{0.95}Co_{0.05}N$	0.1 M KOH	0.5	-	0.76	85 (8)	[11]
Ni_3N/NiO	0.1 M KOH	-	0.95	0.76	90 (20)	[12]
$V_{0.95}Co_{0.05}N$ microflowers	0.1 M KOH	-	0.90	0.80	88 (7)	[17]
$Ni_3FeN/NRGO$	0.1 M KOH	-	0.90	0.75	74 (2)	[18]
$Ti_{0.95}Ni_{0.05}N$	0.1 M KOH	0.5	0.83	0.80	-	[13]
ZrN NPs	0.1 M KOH	1	0.89	0.80	95.6 (36)	[19]
WN/N-C	0.1 M KOH	-	-	$\sim 0.75\ V$	85 (7)	[20]
TiN/TiCN	0.1 M KOH	0.1	0.93	$\sim 0.77\ V$	95 (10)	[21]
Pt/CrN/G	0.1 M KOH	-	0.98	0.87	91.7 (3)	[22]
CrN/rGO	0.1 M KOH	0.1	1.03	0.84	-	[23]
Cr/Z8C	0.1 M KOH	-	-	0.79	-	[24]
Cr ₁₀ Fe ₂ /Z8C	0.1 M KOH	-	-	0.90	89.9 (11)	[24]
CrN/GC	0.1 M KOH	-	0.86	0.70	95.7 (3)	[25]
CrN@NG-900	0.5 M H_2SO_4	0.21	0.90	0.77	86.2 (22)	This work
$Co_{0.5}Mo_{0.5}N_y/NCNCs$	0.5 M H_2SO_4	0.097	0.80	0.58	> 80 (100)	[26]
TiON	0.5 M H_2SO_4	1	-	0.58	-	[27]
FeCoNi-N/CNFs	0.5 M H_2SO_4	0.22	0.73	-	75 (6)	[28]
CoWON/C	0.5 M H_2SO_4	-	0.749	0.5	-	[29]
TiN/CNT-GR	0.5 M H_2SO_4	-	0.83	-	-	[30]

TiN/CB	0.1 M H ₂ SO ₄	-	0.84	-	-	[31]
W ₂ N/XC-72	0.5 M H ₂ SO ₄	0.644	-	0.60	-	[32]
CrN@NG-900	0.1 M HClO₄	0.21	0.92	0.75	82 (24)	This work
Cr/Z8C	0.1 M HClO ₄	-	-	0.72	-	[24]
Cr ₁₀ Fe ₂ /Z8C	0.1 M HClO ₄	-	-	0.76	57.6 (11)	[24]
Ti _{0.95} Ni _{0.05} N	0.1 M HClO ₄	0.5	0.83	0.70	-	[13]
Co _{0.6} Mo _{1.4} N ₂	0.1 M HClO ₄	-	0.71	0.50	-	[33]
Ni _x N	0.1 M HClO ₄	-	0.68	0.49	-	[34]
MoN	0.1 M HClO ₄	-	0.56	-	47 (change in current density) (5)	[35]

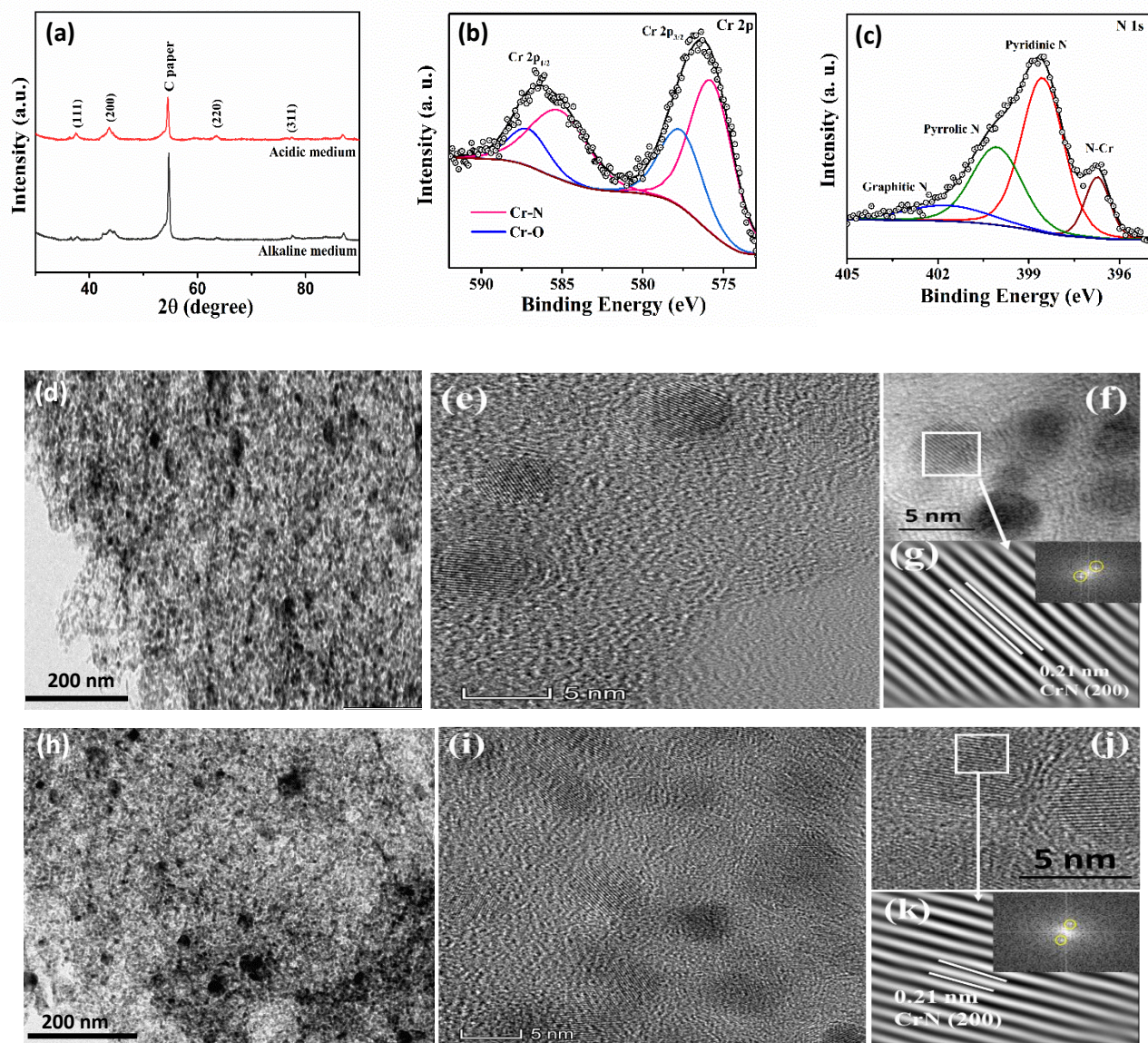


Figure S13. (a) XRD of CrN@NG-900 post-ORR in alkaline and acidic media, HRXPS of (b) Cr 2p and (c) N 1s of CrN@NG-900 post-ORR in acidic media. (d) TEM image, (e, f) HRTEM image, (g) IFFT, inset FFT of CrN@NG-900 post-ORR in alkaline media, (h) TEM image, (i, j) HRTEM image, (k) IFFT, inset FFT of CrN@NG-900 post-ORR in acidic media.

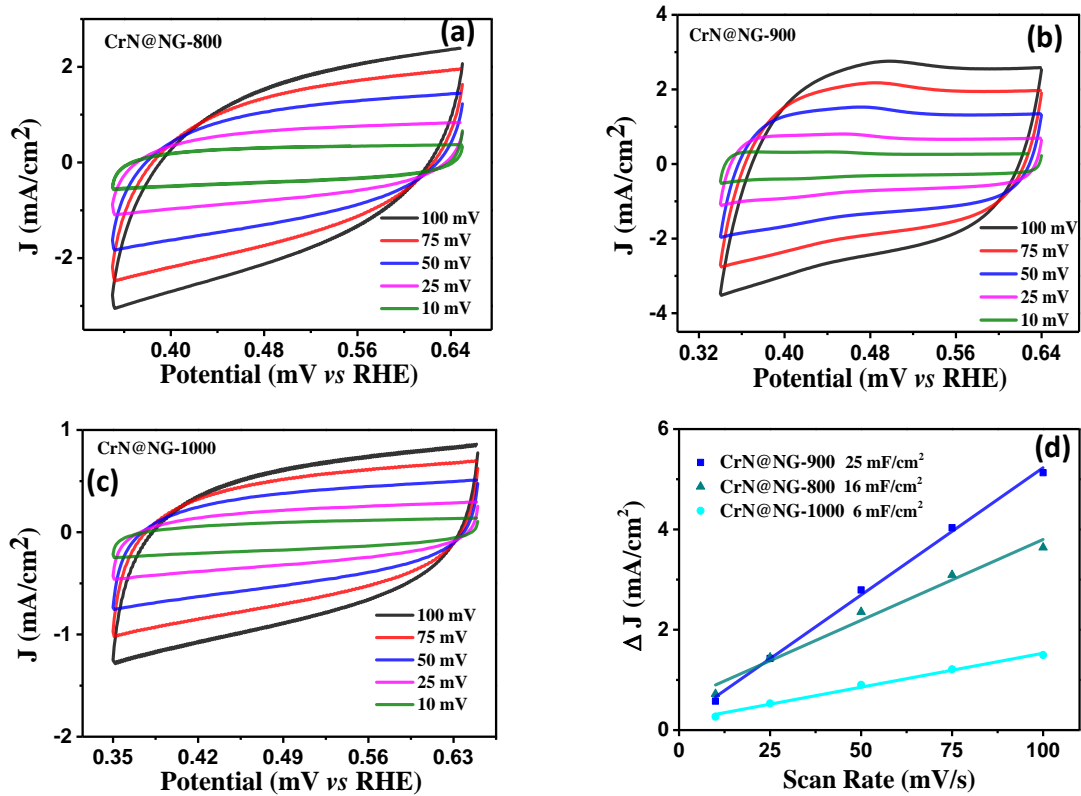


Figure S14. Cyclic voltammetry in the non-faradaic region for (a) CrN@NG-800, (b) CrN@NG-900, (c) CrN@NG-1000 in 0.1 M KOH (d) Double layer capacitance (C_{dl}) plot

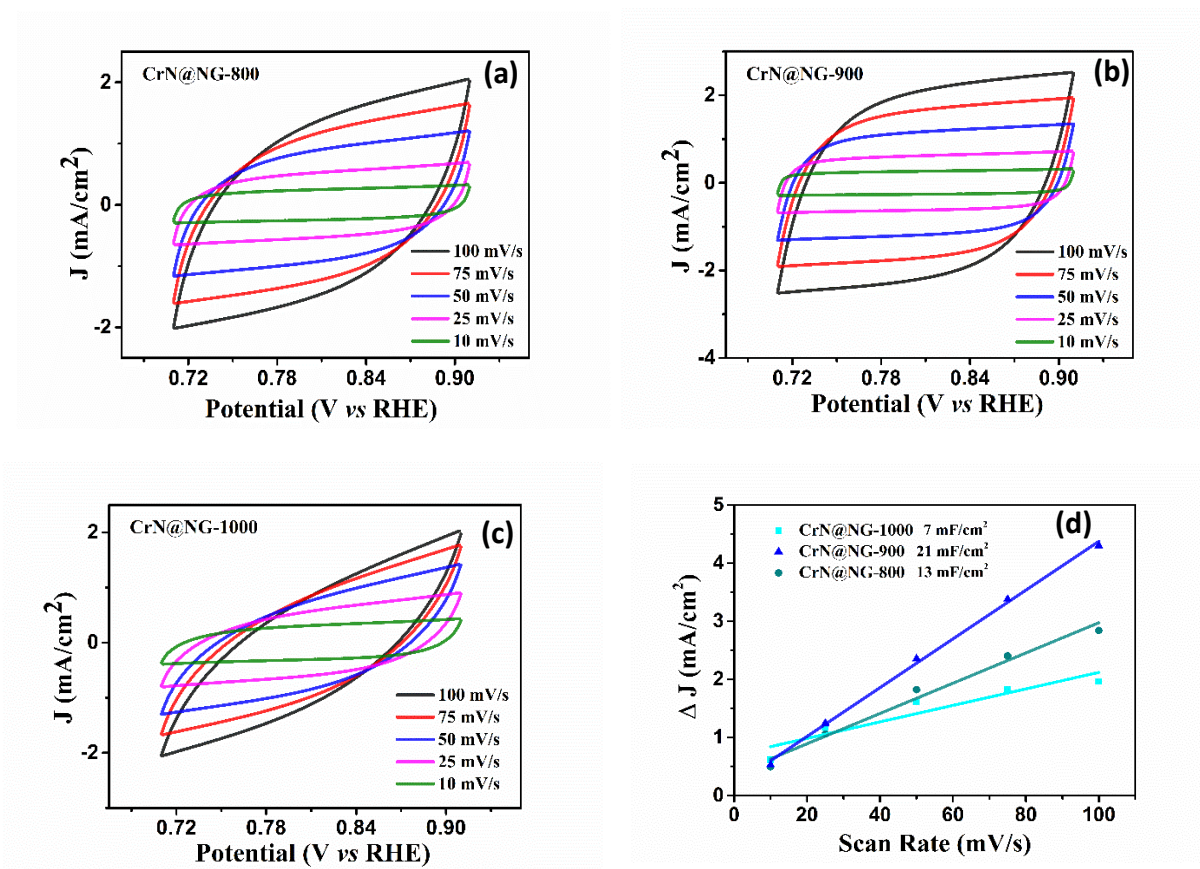


Figure S15. Cyclic voltammetry in the non-faradaic region for (a) CrN@NG-800, (b) CrN@NG-900, (c) CrN@NG-1000 in 0.5 M H_2SO_4 (d) Double layer capacitance (C_{dl}) plot

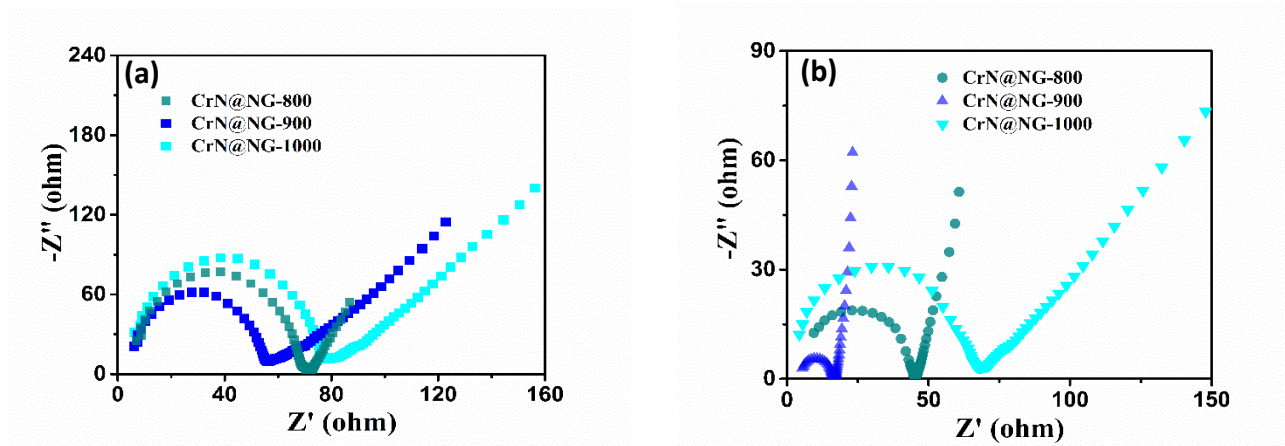


Figure S16. Nyquist plot of the samples in (a) 1 M KOH and (b) 0.5 M H₂SO₄

Table S6 The $R_s + R_{ct}$ values during HER and OER for various catalysts.

	$R_s + R_{ct}$ (ohm)	
	0.1 M KOH	0.5 M H ₂ SO ₄
CrN@NG-800	56.1	44.7
CrN@NG-900	72.4	17.5
CrN@NG-1000	77.6	68

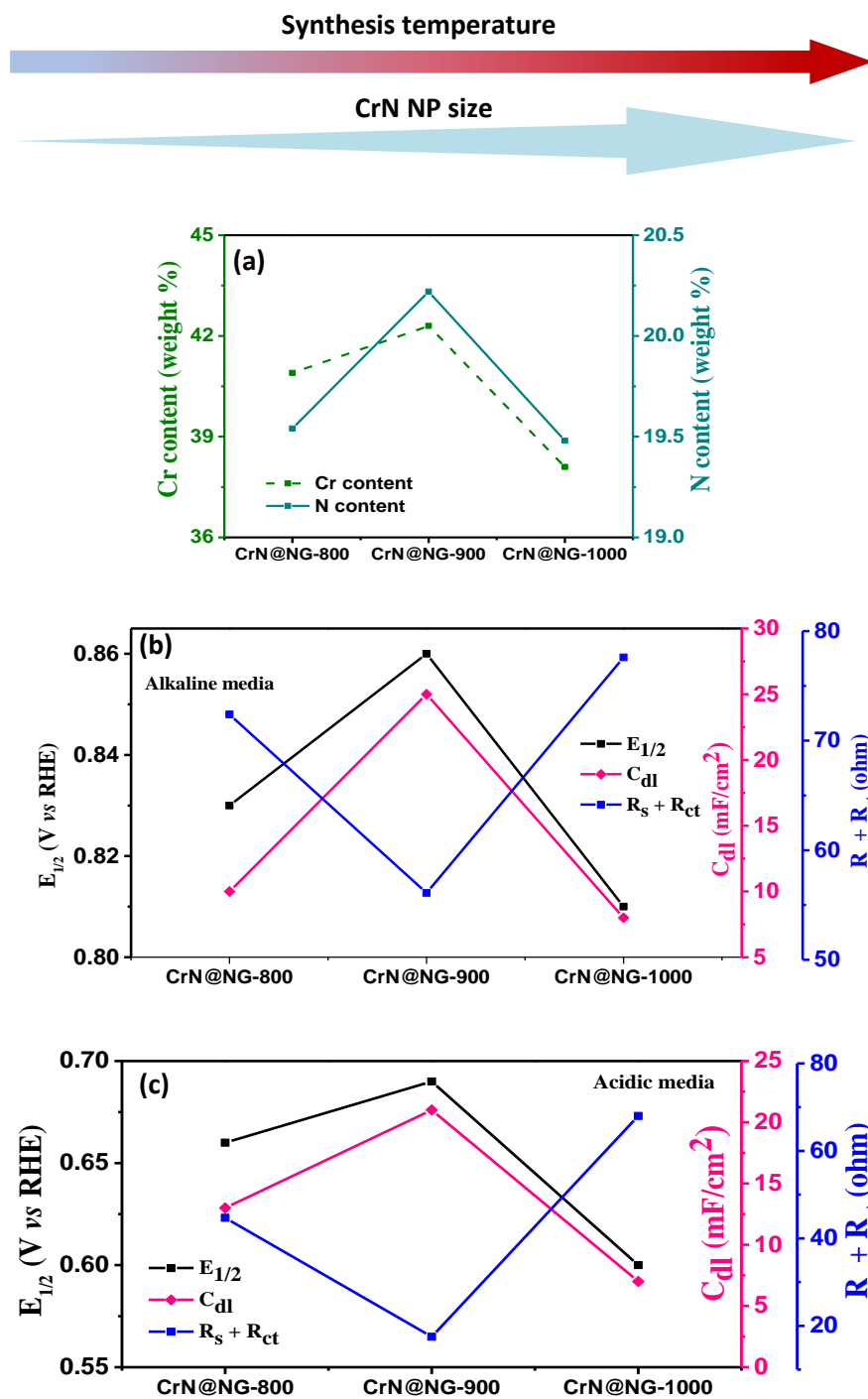


Figure S17. Graphical representation of (a) Cr content (weight % as obtained from ICPMS) and N content (as obtained from EDS), the structure-activity correlation with parameters of $E_{1/2}$, C_{dl} , and $R_s + R_{ct}$ for ORR activity of CrN@NG-T in (b) alkaline media and (c) acidic media

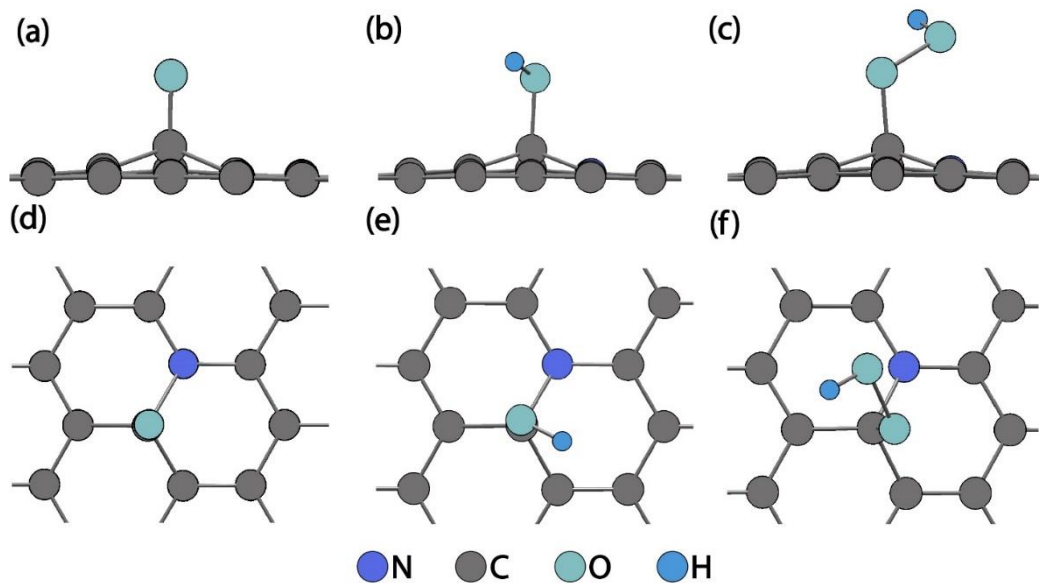


Figure S18. Top view of N-doped carbon (NG) model structure depicting the ORR intermediates adsorbed on the surface. (a) $*O$, (b) $*OH$, (c) $*OOH$ and side view – (d) $*O$, (e) $*OH$, (f) $*OOH$.

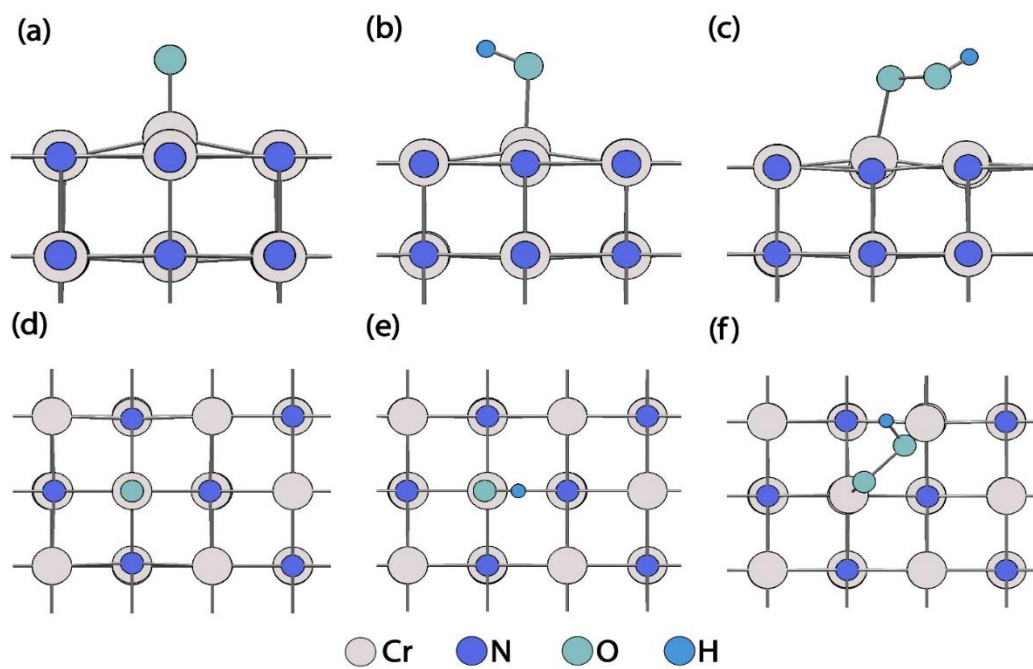


Figure S19. Top view of the model structure of CrN depicting the ORR intermediates adsorbed on the surface. (a) $*O$, (b) $*OH$, (c) $*OOH$ and side view – (d) $*O$, (e) $*OH$, (f) $*OOH$.

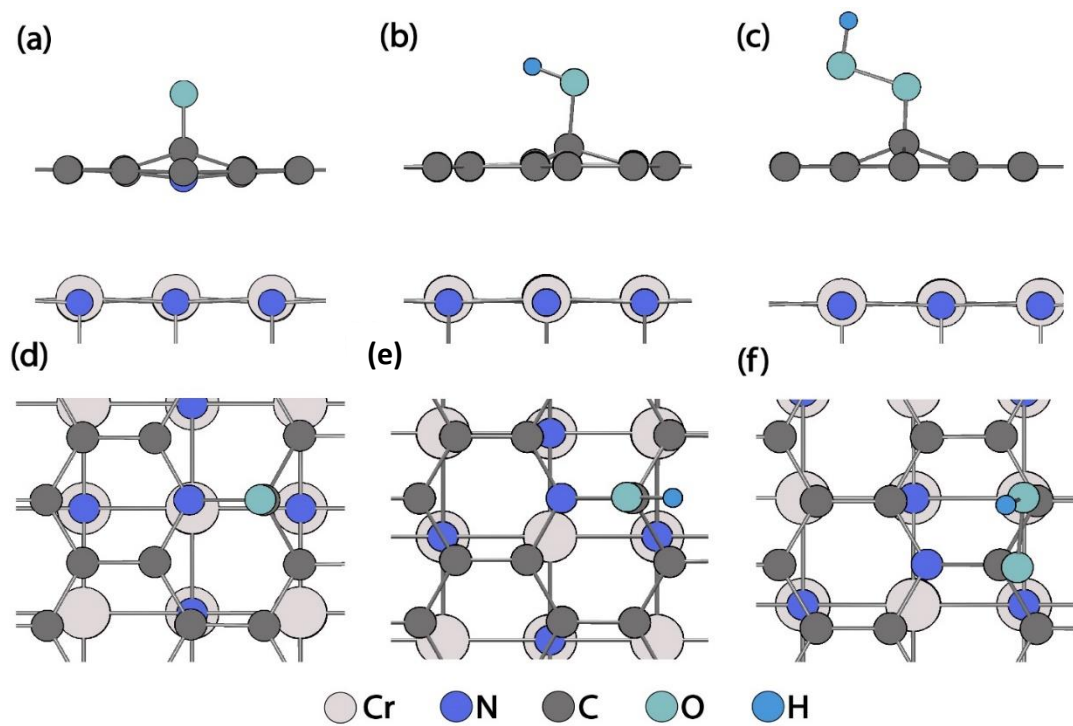


Figure S20. Top view of the model structure of CrN@NG[#] depicting the ORR intermediates adsorbed on the surface. (a) *O, (b) *OH, (c) *OOH and side view – (d) *O, (e) *OH, (f) *OOH.

References

- [1] W. Kiciński, S. Dyjak, *Carbon* **2020**, *168*, 748-845.
- [2] C. Ge, F. Lao, W. Li, Y. Li, C. Chen, Y. Qiu, X. Mao, B. Li, Z. Chai, Y. Zhao, *Analytical Chemistry* **2008**, *80*, 9426-9434.
- [3] Y. Zhou, S. Xi, J. Wang, S. Sun, C. Wei, Z. Feng, Y. Du, Z. J. Xu, *ACS Catalysis* **2018**, *8*, 673-677.
- [4] R. Nandan, A. Gautam, K. K. Nanda, *Journal of Materials Chemistry A* **2018**, *6*, 20411-20420.
- [5] G. Kresse, J. Hafner, *Physical Review B* **1993**, *47*, 558-561.
- [6] G. Kresse, D. Joubert, *Physical Review B* **1999**, *59*, 1758-1775.
- [7] J. P. Perdew, K. Burke, M. Ernzerhof, *Physical Review Letters* **1996**, *77*, 3865-3868.
- [8] S. L. Dudarev, G. A. Botton, S. Y. Savrasov, C. J. Humphreys, A. P. Sutton, *Physical Review B* **1998**, *57*, 1505-1509.
- [9] L. Lindsay, D. A. Broido, *Physical Review B* **2010**, *81*, 205441.
- [10] B. Cao, G. M. Veith, R. E. Diaz, J. Liu, E. A. Stach, R. R. Adzic, P. G. Khalifah, *Angewandte Chemie International Edition* **2013**, *52*, 10753-10757.
- [11] J. Luo, X. Tian, J. Zeng, Y. Li, H. Song, S. Liao, *ACS Catalysis* **2016**, *6*, 6165-6174.
- [12] H. Zhang, M. Liu, W. Cheng, Y. Li, W. Zhou, H. Su, X. Zhao, P. Yao, Q. Liu, *The Journal of Physical Chemistry C* **2019**, *123*, 8633-8639.
- [13] X. Tian, J. Luo, H. Nan, Z. Fu, J. Zeng, S. Liao, *Journal of Materials Chemistry A* **2015**, *3*, 16801-16809.
- [14] X. Zhang, C. Chen, J. Dong, R.-X. Wang, Q. Wang, Z.-Y. Zhou, S.-G. Sun, *ChemElectroChem* **2018**, *5*, 3946-3952.
- [15] C. H. Choi, S. H. Park, S. I. Woo, *ACS Nano* **2012**, *6*, 7084-7091.
- [16] P. Chandran, A. Ghosh, S. Ramaprabhu, *Scientific Reports* **2018**, *8*, 3591.
- [17] H. Tang, J. Luo, X. L. Tian, Y. Dong, J. Li, M. Liu, L. Liu, H. Song, S. Liao, *ACS Applied Materials & Interfaces* **2018**, *10*, 11604-11612.
- [18] Y. Fan, S. Ida, A. Staykov, T. Akbay, H. Hagiwara, J. Matsuda, K. Kaneko, T. Ishihara, *Small* **2017**, *13*, 1700099.
- [19] Y. Yuan, J. Wang, S. Adimi, H. Shen, T. Thomas, R. Ma, J. P. Attfield, M. Yang, *Nature Materials* **2020**, *19*, 282-286.
- [20] Y. Dong, J. Li, *Chemical Communications* **2015**, *51*, 572-575.
- [21] Z. Jin, P. Li, D. Xiao, *Scientific reports* **2014**, *4*, 6712-6712.
- [22] B. Liu, L. Huo, R. Si, J. Liu, J. Zhang, *ACS Applied Materials & Interfaces* **2016**, *8*, 18770-18787.
- [23] K. Khan, A. K. Tareen, M. Aslam, Q. Khan, S. A. Khan, Q. U. Khan, A. S. Saleemi, R. Wang, Y. Zhang, Z. Guo, H. Zhang, Z. Ouyang, **2019**, *7*.
- [24] J. Luo, X. Qiao, J. Jin, X. Tian, H. Fan, D. Yu, W. Wang, S. Liao, N. Yu, Y. Deng, *Journal of Materials Chemistry A* **2020**, *8*, 8575-8585.
- [25] L. Zhao, L. Wang, P. Yu, D. Zhao, C. Tian, H. Feng, J. Ma, H. Fu, *Chemical Communications* **2015**, *51*, 12399-12402.
- [26] T. Sun, Q. Wu, R. Che, Y. Bu, Y. Jiang, Y. Li, L. Yang, X. Wang, Z. Hu, *ACS Catalysis* **2015**, *5*, 1857-1862.
- [27] M. Chisaka, Y. Ando, N. Itagaki, *Journal of Materials Chemistry A* **2016**, *4*, 2501-2508.
- [28] Q. Liu, S. Cao, Y. Fu, Y. Guo, Y. Qiu, *Journal of Electroanalytical Chemistry* **2018**, *813*, 52-57.
- [29] T. Ando, S. Izhar, H. Tominaga, M. Nagai, *Electrochimica Acta* **2010**, *55*, 2614-2621.
- [30] D. H. Youn, G. Bae, S. Han, J. Y. Kim, J.-W. Jang, H. Park, S. H. Choi, J. S. Lee, *Journal of Materials Chemistry A* **2013**, *1*, 8007-8015.
- [31] J. Chen, K. Takanabe, R. Ohnishi, D. Lu, S. Okada, H. Hatasawa, H. Morioka, M. Antonietti, J. Kubota, K. Domen, *Chemical Communications* **2010**, *46*, 7492-7494.

- [32] H. Zhong, H. Zhang, Y. Liang, J. Zhang, M. Wang, X. Wang, *Journal of Power Sources* **2007**, *164*, 572-577.
- [33] B. Cao, J. C. Neuefeind, R. R. Adzic, P. G. Khalifah, *Inorganic Chemistry* **2015**, *54*, 2128-2136.
- [34] M. E. Kreider, A. Gallo, S. Back, Y. Liu, S. Siahrostami, D. Nordlund, R. Sinclair, J. K. Nørskov, L. A. King, T. F. Jaramillo, *ACS Applied Materials & Interfaces* **2019**, *11*, 26863-26871.
- [35] M. E. Kreider, M. B. Stevens, Y. Liu, A. M. Patel, M. J. Statt, B. M. Gibbons, A. Gallo, M. Ben-Naim, A. Mehta, R. C. Davis, A. V. Ievlev, J. K. Nørskov, R. Sinclair, L. A. King, T. F. Jaramillo, *Chemistry of Materials* **2020**, *32*, 2946-2960.